RADIALcvt prototype design and simulation

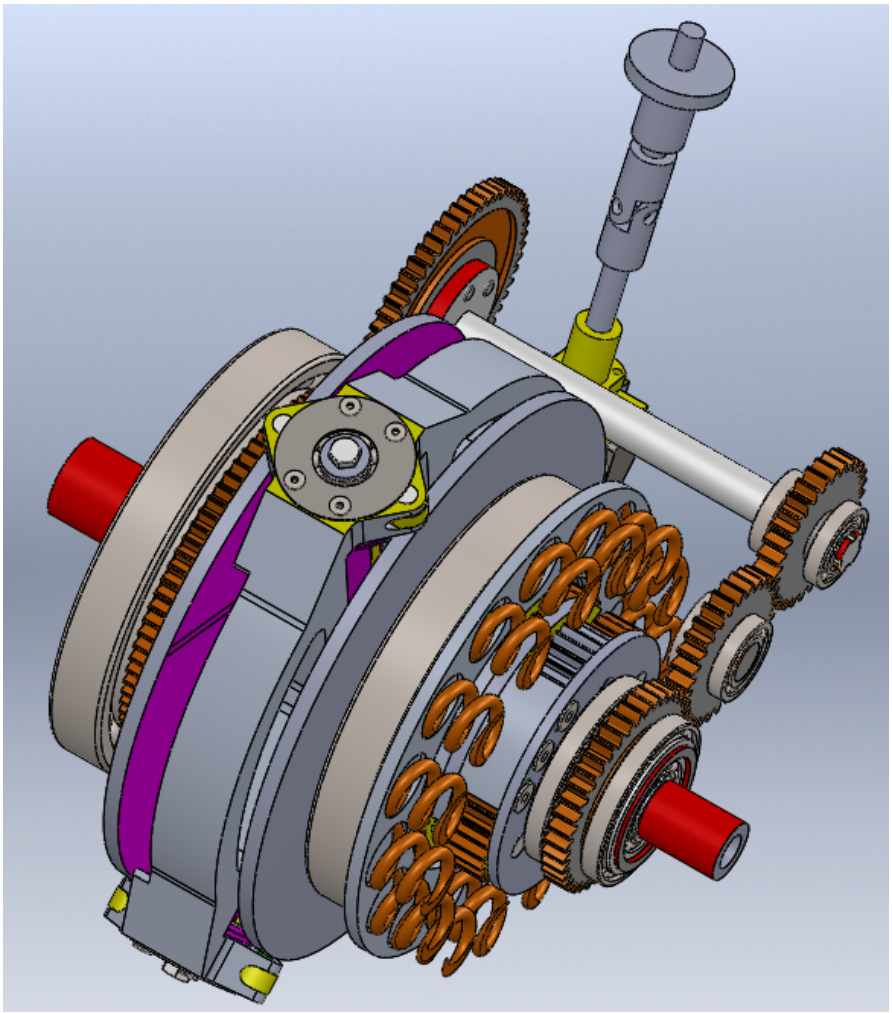

Dr. J. J. Naude

22 May 2017

Version 1.6

Table of contents

1 Executive summary 4

2 RADIALcvt specifications 5

3 Traction drive simulation 7

3.1 Geometry angles 7

3.2 Geometry radiusses 8

3.3 Operating parameters 10

3.4 Matlab simulation steps 11

4 Matlab simulation results 18

4.1 Traction curves, spin and max traction coefficient 19

4.2 Elliptic ratio, maximum contact stress and power efficiency 22

4.3 Comments on optimization 24

4.3.1 Increasing maximum disk size 24

4.3.2 Varying planetary system e value 25

4.3.3 Integrating a two speed AMT 25

4.3.4 Increase line contact length 26

4.3.5 Different Θ angles and a loading cam 27

5 Contact simulation summary 28

5.1 Without AMT integration 28

5.2 With 2 speed AMT integration 28

6 Bearing loss analysis 30

6.1 Disk bearings 30

6.1.1 Clamping force advantages 32

6.2 Radial shaft bearing losses 33

7 Ratio shifting analysis 34

7.1 Geometry analysis 34
7.2 Total shifting torque and forces 37
8 References 37

List of Figures

Figure 1. 3D CAD design of the RADIALcvt prototype 6
Figure 2 Geometry in the y-plane 7
Figure 3 Body A and B configuration 8
Figure 4 Geometry in the x-plane 9
Figure 5 Surface velocity vs maximum traction coefficient 11
Figure 6 Regression coefficients (Loewenthal & Zaretsky, 1985) page 35 13
Figure 7 Regression analysis parameter ranges 17
Figure 8 Traction curves 19
Figure 9 Spin and maximum traction coefficient 20
Figure 10 Power efficiency and power losses 20
Figure 11 Maximum contact stress and elliptic ratio 22
Figure 12 Power efficiency and Input torque 23
Figure 13 Input power, torque and power efficiency for the complete RADIALcvt 24
Figure 14 Minimum surface roughness and EHD film thickness 24
Figure 15 Effect of 2 speed AMT integration 25
Figure 16 Effect of 2 speed AMT integration and line contact length increase 26
Figure 17 Line contact increase effect on spin and maximum traction coefficient. 27
Figure 18 Disk bearing loss: AMT integrated and extended contact line. 31
Figure 19 Disk bearing loss: Basic case without AMT integration. 32
Figure 20 Bottom radial driver bearing losses. 33
Figure 21 Radial driver force diagram 34
Figure 22 Radial shaft and driver 35
Figure 23 Ratio shifting forces 36

1 Executive summary

This document provides a design and traction drive contact analysis and simulation of the first RADIALcvt prototype. The simulation results are discussed and improvements to the current design recommended. It presents a high mechanical efficiency and eliminates the use of a hydraulic control system. The RADIALcvt has a number of fundamental advantages that sets it apart from all other developmental and commercial CVT's and are listed below:

- **One friction interface:** Only one friction drive interface in series in a parallel power path. All other CVT's, developmental and commercial have 2 friction drive interfaces in series thus resulting in a compound friction loss. Thus if the friction contacts have the same efficiency then the RADIALcvt will have 50% of the friction drive losses of other CVT's. See section 4 and 5 for details.
- **Line contact:** The friction drive contact in the RADIALcvt friction drive can be a line contact, which is only possible in belt/chain CVT and cone ring CVT and not possible in toroidal and planet ball CVT's. Line contact reduces the maximum contact stress.
- **Constant input radius:** The RADIALcvt has a constant friction drive input radius. All other CVT have a variable input radius which results in high surface rolling speeds and lower coefficient of friction which require higher clamping forces. See section 4.
- **Six parallel power paths:** The RADIALcvt has at least 6 parallel power paths. Such a large number of parallel paths is only possible in planet ball CVT's.
- **Large output friction disk:** The output friction drive disk of the RADIALcvt can be positioned concentric and close to the engine flywheel and can approximate flywheel size. Thus the diameter of this output friction drive can be much larger than any of the belt/chain or toroidal or cone ring CVT output friction drive components. Due to this fact the RADIALcvt provides its highest efficiency in low ratios associated with city driving. See section 4 and 5 for details.
- **High power efficiency:** Above results in a RADIALcvt with a friction drive contact power efficiency in all ratios, under maximum engine torque, of about 95% in high ratio to about 98% in low ratio including in use, without a 2 speed AMT, with a ratio range up to 4.7, or with ratio range up to 10 and beyond with 2 speed AMT integration. A ratio range of 10 is currently the maximum in the industry. See section 4 and 5 for details.

- **No hydraulic control:** As shown in section 4 and 5, the RADIALcvt can be realised without any hydraulic control. All current developmental and commercial CVT require a hydraulic control system.
- **Clamping force utilization:** In the RADIALcvt configuration, a unit of clamping force supports two parallel friction drive interfaces, while in all other developmental and commercial CVT's only one friction drive interface is supported. Losses due to clamping forces should thus be 50% lower in the RADIALcvt. See section 5 for details.
- **Clamping force location:** The RADIALcvt clamping force, bearing losses are only associated with the RADIALcvt output, namely the Convex and Concave disks, while the RADIALcvt input, the radial drivers, are in equilibrium as mentioned in section 4.3.5. Thus these bearing losses, for a given clamping force, are only a function of the RADIALcvt output speed. This has the obvious low loss advantages in low output speed ratios. In contrast in all other CVT's, the clamping force is associated with both the input and output speeds of the respective CVT, thus for a given clamping force the applicable speed for bearing loss calculation would be the average of the input and output speeds.
- **Low bearing losses:** Disk bearing (clamping) losses, which are a well-known source of traction drive losses (Loewenthal & Zaretsky, 1985), are a maximum of 2.5% in high ratio to about 1.5% in low ratio of transmitted power. See section 6 for details.

Since the RADIALcvt use existing very well developed traction/ friction drive technology, any potential licensee of our technology can very easily evaluate and verify the advantages of the RADIALcvt. The advantages of the RADIALcvt is realised by its unique patented configuration of components.

2 RADIALcvt specifications

The RADIALcvt presented in this document functions according to the PCT patent application number PCT/ZA2016/050017. The current prototype has the following specifications:

- Input torque 70 N.m (extended to 225 N.m with AMT integration)
- Maximum input rpm 4400

- Disk diameter 292 mm
- Width 262mm
- Height 340 mm

Figure 1 presents a 3D CAD design of the RADIALcvt prototype. Note that in this design the combining planetary system is integrated in the rear of the rear convex disk, while in PCT/ZA2016/050017 it is positioned to one side. This design used the same variator configuration as in PCT/ZA2016/050017 that is with 3 radial drivers, making contact and driving the two disks in opposite directions in a traction fluid. Thus 6 traction drive contact points are created, representing the 6 parallel power paths, each parallel path containing only one friction drive interface in series.

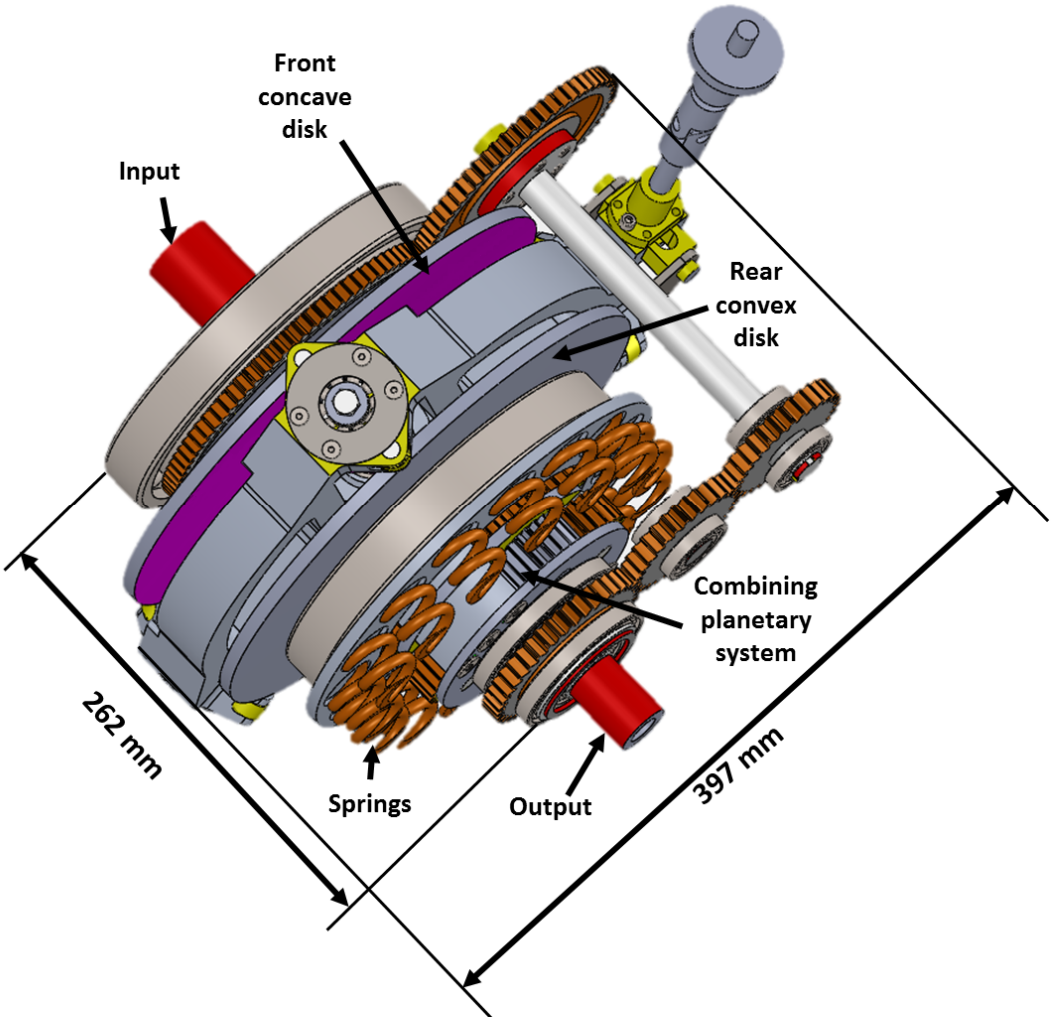

Figure 1. 3D CAD design of the RADIALcvt prototype

3 Traction drive simulation

This section presents the simulation of the traction drive interface of a radial driver clamped between the convex and concave disk. This simulation is based on the design methodology as presented in (Loewenthal & Zaretsky, 1985). This work is based on regression analysis of a large number of experimental results using Santotrac 50 and TDF 88 as traction fluid. This methodology was also recently used, among others, by (Lichao, 2013) and (Carter, Pohl, Raney, & Sadler, 2004).

3.1 Geometry angles

Figure 2 presents the geometry of a driver clamped between disks in the y plane. The y direction is defined as the direction away from the coincident axes of rotation of body B (convex disk) and body C (concave disk). The notation used is the same as used in (Loewenthal & Zaretsky, 1985) page 26 and 27.

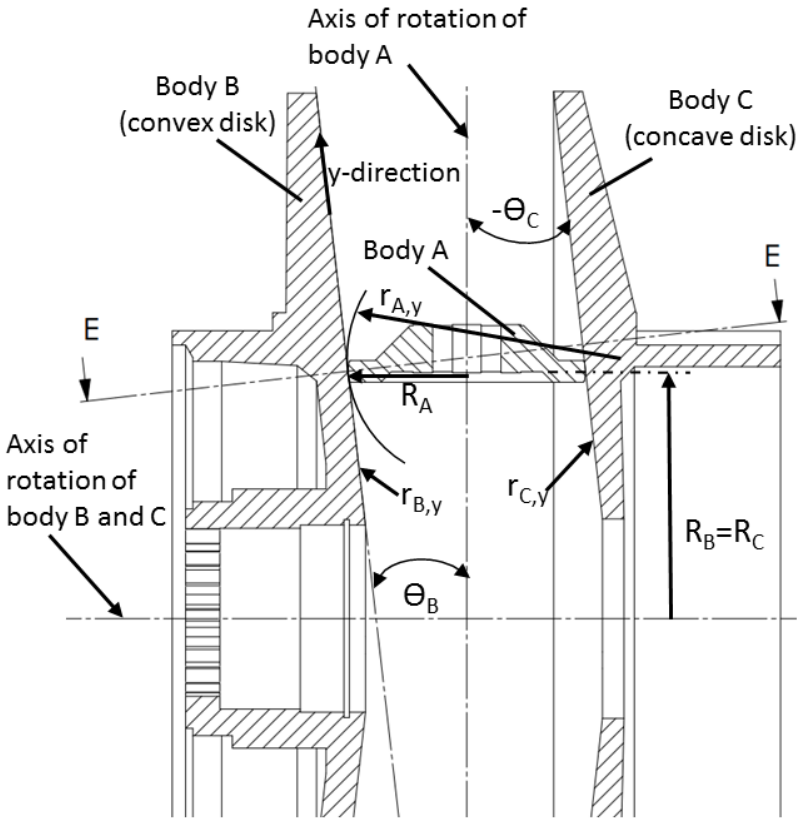

Figure 2 Geometry in the y-plane

Considering body A and B, the angle γ is defined as the angle between the axes of rotation of body A and B and is 90^0. Similarly γ for bodies A and C is also 90^0. Considering body A and B, the angle Θ is defined as the angle between the rotation axis of body A and the line/plane tangent to the contact point. Θ_B refers to the interface between body A and B and Θ_C refers to the interface between body A and C. In the current RADIALcvt design the convex disk and concave disk have the same disk angle of 6.5^0.

Figure 3 below presents Figure 25 of (Loewenthal & Zaretsky, 1985) as it is used to determine Θ for different traction drive configurations. From Figure 3 it is concluded that for the body A and B interface (most left configuration in the 3rd row) $\Theta_B=6.5^0$ and for body A and C interface (most left configuration in the 4th row) $\Theta_C=-6.5^0$. Note that in Figure 3 body A rotates around the horizontal axis

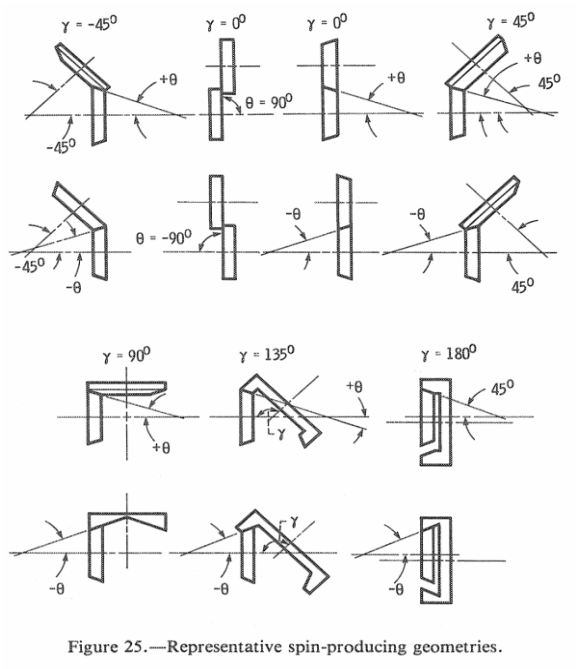

Figure 25.—Representative spin-producing geometries.

Figure 3 Body A and B configuration

3.2 Geometry radiusses

Figure 4 presents a view of section E-E in Figure 2 which also presents the x direction/plane. The x-direction is defined as the rolling direction.

The following are the relevant radiuses and their values and value ranges of the current RADIALcvt prototype:

Body A

R_A=31 mm	Rolling radius of body A
$R_{A,x}$=31 mm	Contact radius of body A in the x direction
$R_{A,y}$=45 mm	Contact radius (crown) of body A in the y direction. This contact is also modelled as line contact in which case it has infinite value.
$R_{A,yline}$=2.35mm	In the case where $R_{A,y}$ is modelled as a line contact, this value refers to the length of the line contact.

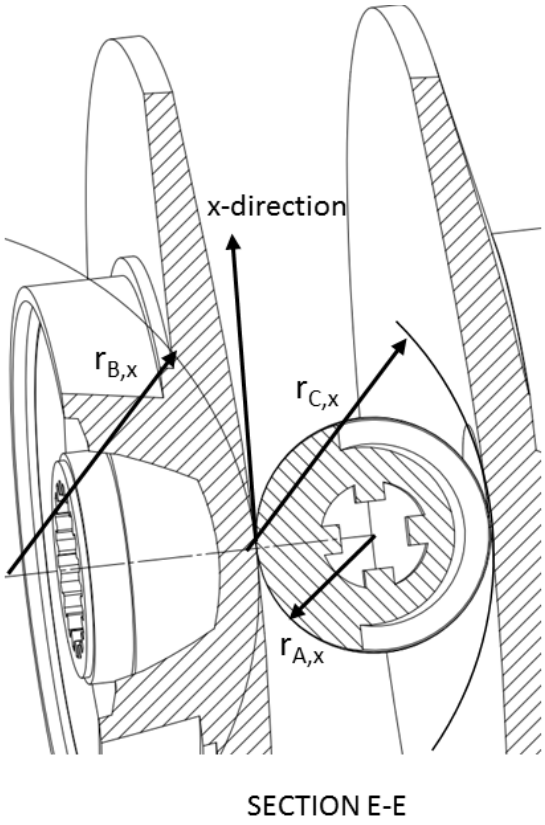

Figure 4 Geometry in the x-plane

Body B

R_B=30 - 143 mm	Variable rolling radius of body B
$R_{B,x}$	Contact radius of body B in the x-direction which is a function of R_B. $R_{B,x}$ is calculated by a Matlab function calculating the projected circle created by R_B projected on a plane tilted at an angle equal to the disk angle.

$R_{B,y}$=infinity	Contact radius of body B in the y direction. This contact is a line contact, thus the infinite value.

Body C

R_C=30 - 143 mm	Variable rolling radius of body C
$R_{C,x}$	Contact radius of body C in the x direction which is a function of R_C. Note that $R_{C,x}$= -$R_{B,x}$ because of the negative radius. (Convex vs Concave)
$R_{C,y}$=infinity	Contact radius of body C in the y direction. This contact is a line contact, thus the infinite value.

During simulation R_B and R_C are varied, which caused $R_{C,x}$ and $R_{B,x}$ to vary while all the other above angles and radiuses are kept constant.

3.3 Operating parameters

The current RADIALcvt is intended as a hydraulic free CVT for small passenger vehicles, typically around 70 N.m, 40 kW torque and power. In these vehicles there is no need to operate the engine above 4400 rpm as at this point maximum power is achieved while maximum torque is achieved at lower rpm. Thus 4400 rpm is taken as the input speed and also the speed of the drivers (body A). The normal load, Q, in the traction contact is taken as 6800 N. The surface rolling speed in the x-direction, U, is calculated as U=4400 rpm*pi*2*R_A/60=14.3 m/s. Note that since the radius R_A=31 mm of body A does not change, U is also a constant, which is not the case in current commercial CVT or CVT's in development including, Cone ring, Toroidal and Planet ball CVT's. The fact that U is constant for the RADIALcvt is a huge advantage, because as U increases, the maximum traction coefficient decreases as reported by (Loewenthal & Rohn, 1983) figure 11 , duplicated below as Figure 5.

The low maximum surface velocity, U=14.3 m/s, of the RADIALcvt prototype will thus contribute to a higher maximum traction coefficient. Figure 5 also indicates that maximum contact pressures above about 2 GPa do not increase the maximum traction coefficient. The lubricant inlet temperature is set at $\tilde{T}$ = 50 ^{0}C.

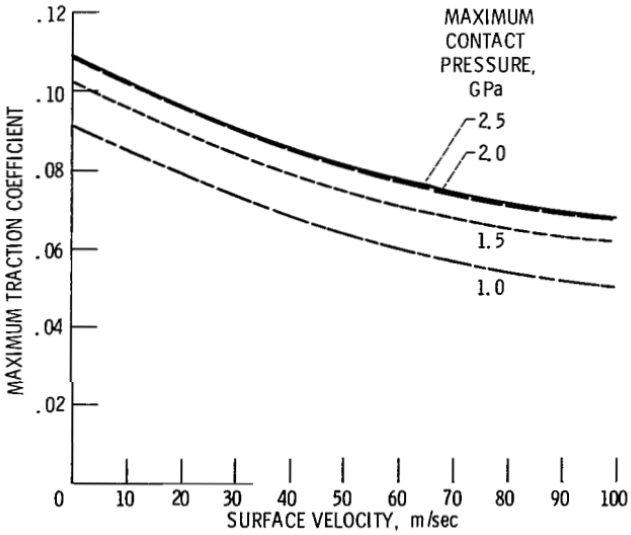

Figure 11. - Effect of surface velocity on maximum traction coefficient. Predicted from Santotrac 50 correlation. Temperature, 80° C; ellipticity ratio, 5; zero spin.

Figure 5 Surface velocity vs maximum traction coefficient

3.4 Matlab simulation steps

The below section describes the sequence of calculations performed in the Matlab contact simulation.

a) Calculate equivalent radii

$$\frac{1}{R_x} = \frac{1}{r_{A,x}} + \frac{1}{r_{B,x}}$$

(Loewenthal & Zaretsky, 1985) equation 3

$$\frac{1}{R_y} = \frac{1}{r_{A,y}} + \frac{1}{r_{B,y}}$$

(Loewenthal & Zaretsky, 1985) equation 10

b) Calculate contact parameters

$$\rho = \frac{1}{R_x} + \frac{1}{R_y}$$

Inverse curvature sum (Loewenthal & Zaretsky, 1985) equation 17

$$g = \sqrt[3]{\frac{3Q}{2\rho}\left(\frac{1-\xi_A^2}{E_A} + \frac{1-\xi_B^2}{E_B}\right)}$$

Auxiliary contact size parameter (Loewenthal & Zaretsky, 1985) equation 16

Where $E_A = E_B = 207$ GPa representing the modulus of elasticity of steel and $\xi_A = \xi_B = 0.3$ representing the poison ratio for steel.

$$k = \left(\frac{R_y}{R_x}\right)^{2/\pi}$$

Elliptic ratio (Loewenthal & Zaretsky, 1985) equation 9

Figure 11 in (Loewenthal & Zaretsky, 1985) was digitised and used as a lookup for dimensionless contact ellipse factors a^* and b^* using k.

The contact elliptic radii are calculated as:

$$a = a^* g; \quad b = b^* g$$

Elliptic ratio (Loewenthal & Zaretsky, 1985) equation 14

c) Maximum contact stress

The maximum contact stress is calculated as:

$$\sigma_0 = \frac{3Q}{2\pi ab}$$

Maximum contact stress (Loewenthal & Zaretsky, 1985) equation 14

As a comparison, the maximum contact stress, σ_0, b and k are also calculated for Hertz cylinder-cylinder contact where $R_{A,yline}$=2a, while b and σ_0 is calculated via the Hertz formula and k from k=a/b.

d) Calculate spin, maximum traction coefficient and initial traction slope

Spin, ω_S, is the result of a mismatch in roller radii at contact points on either side of the point of pure rolling and is calculated by:

$$\frac{\omega_S}{U} = \frac{\sin\theta}{R_A} - \frac{\sin(\gamma - \theta)}{R_B}$$

(Loewenthal & Zaretsky, 1985) equation 36

Non dimensional spin is calculated as:

$$\omega_S \sqrt{ab}/U$$

(Loewenthal & Zaretsky, 1985) page 35

Use the regression results to calculate the maximum available traction coefficient, μ and the initial slope of the traction curve, m.

$$\mu = C_1 + C_2\sigma_0 + C_3\sigma_0^2 + C_4 U + C_5 U^2 + C_6 \tilde{T} + C_7 k + C_8 \frac{\omega_S \sqrt{ab}}{U}$$

(Loewenthal & Zaretsky, 1985) equation 52

$$m = C_1 + C_2\sigma_0 + C_3 \ln \sigma_0 + C_4 U + C_5 U^2 + C_6 \tilde{T} + C_7 k$$

Where the coefficients are presented in below table:

TABLE III.—CORRELATION COEFFICIENTS FOR SANTOTRAC-50 AND TDF-88

Coefficient	Santotrac-50	TDF-88	Santotrac-50	TDF-88
	Initial slope, m		Maximum traction coefficient, μ	
C_1	101.4	51.3	0.0726	0.0733
C_2	−45.49	−6.53	.0477	.0443
C_3	69.44	17.20	−.0102	−.0116
C_4	−.289	−.646	-6.92×10^{-4}	-7.36×10^{-4}
C_5	1.30×10^{-3}	4.99×10^{-3}	2.47×10^{-6}	2.38×10^{-6}
C_6	6.63×10^{-2}	.236	-2.13×10^{-4}	-9.08×10^{-5}
C_7	−2.99	−1.24	-3.41×10^{-4}	-1.88×10^{-3}
C_8	----------	----------	−1.22	−.443

Figure 6 Regression coefficients (Loewenthal & Zaretsky, 1985) page 35

Slope correction on m is performed by:

$$\frac{m^*}{m}=\left\{\left(\frac{R_x}{R_x^*}\right)^{0.67}+7.66\times10^{-3}m\sigma_0 e^{-0.21/k}\times\left[1-A\left(\frac{R_x}{R_x^*}\right)^{0.67}\right]^{-1}\right\}$$

(Loewenthal & Zaretsky, 1985) equation 53

Where $A=1.43-0.383/k+0.0995/k2$ and R_x^*=22.57mm for Santotrac 50 and 12.5mm for TDF-88.

The dimensionless spin parameter J_3, is calculated as:

$$J_3=C\frac{\omega_s\sqrt{ab}}{U}$$

(Loewenthal & Zaretsky, 1985) equation 39

Where $C=\frac{3\pi}{8}\frac{m}{\mu}\sqrt{k}$

(Loewenthal & Zaretsky, 1985) equation 44

e) Slip/creep calculations

Slip or creep is the differential velocity, ΔU, in the rolling direction (x- direction) arising from the shear forces generated between body A and B across the lubricant film. If no slip exists, there is no traction and the coefficient of friction in the x-direction μ_x=0. It is therefore important to generate the relationship between ΔU and μ_x as ΔU increases while μ_x also increases to its maximum value. The graph

detailing ΔU/U versus μ_X is used for this purpose and is referred to as the traction curve. In order to generate the traction curve, incremental values for ΔU/U from 0 to 0.07 (0% to 7%) is generated and the following is performed for each increment to calculate the respective μ_X value as well as traction in the y-direction, μ_Y value:

Dimensionless J_1 parameter is calculated as:

$$J_1 = C\frac{\Delta U}{U}$$

(Loewenthal & Zaretsky, 1985) equation 37

Figure 27 in (Loewenthal & Zaretsky, 1985) was digitised and used as a lookup for dimensionless traction in the x-direction parameter J_4 by using above J_1 and previously calculated J_3 and k values.

μ_X is now calculated from:

$$J_4 = \frac{\mu_x}{\mu}$$

(Loewenthal & Zaretsky, 1985) equation 40

Spin also generates a side traction force and this need to be calculated.

Figure 30 in (Loewenthal & Zaretsky, 1985) was digitised and used as a lookup for dimensionless side traction in the y-direction parameter J_5 by using above J_1 and previously calculated J_3 value.

μ_Y is now calculated from:

$$J_5 = \frac{\mu_y}{\mu}$$

(Loewenthal & Zaretsky, 1985) equation 41

By repeating above for each ΔU/U increment the traction curve can be plotted.

f) Selecting operating μ_X

Usually μ_X selected for operating conditions is a percentage of the maximum available μ_X value in the traction curve. For the purposes of this simulation the operating μ_X is set to 90% of the value of μ_X at 5% slip on the traction curve and the corresponding J_4 value is calculated as:

$$J_4 = \frac{\mu_x}{\mu}$$

(Loewenthal & Zaretsky, 1985) equation 40

Where μ_X now represents the value of μ_X under operating conditions at 5% slip level.

g) Power calculations

Transmitted power and torque

The transmitted power Pt is calculated as:

$P_t = \mu_X QU$ (Loewenthal & Zaretsky, 1985) page 3

The transmitted input torque is calculated as:

$T_t = 60P_t/(2\pi \text{input rpm})$

Power traction contact loss

Figure 31 in (Loewenthal & Zaretsky, 1985) was digitised and used as a lookup for the power loss factor LF by using the above calculated values for J_4, J_3 and k.

The ratio of $\left(\frac{\text{Power loss}}{\text{Power input}}\right)$ for the contact loss can now be calculated from:

$$\text{LF} = \frac{J_7}{J_4} = C\left(\frac{\text{Power loss}}{\text{Power input}}\right)$$

(Loewenthal & Zaretsky, 1985) equation 45

The traction contact power loss is calculated as:

$P_C = \left(\frac{\text{Power loss}}{\text{Power input}}\right) P_t$

Rolling traction power loss

By estimating the central EHD film thickness, the power loss due to rolling of the traction contact can be determined.

The material elastic parameter is calculated as:

$$E' = \frac{2}{\left(\frac{1-\xi_A^2}{E_A} + \frac{1-\xi_B^2}{E_B}\right)}$$

(Loewenthal & Zaretsky, 1985) equation 6

The dimensionless EHD speed parameter is calculated as:

$$U_D = \frac{\eta_0 U}{E' R_x}$$ (Loewenthal & Zaretsky, 1985) equation 4

Where η_0 =0.0194 represents the absolute viscosity of the traction fluid (Santotrac 50) at ambient pressure.

The dimensionless EHD load parameter is calculated as:

$$W = \frac{Q}{E' R_x^2}$$ (Loewenthal & Zaretsky, 1985) equation 7

The dimensionless EHD materials parameter is calculated as:

$$G = \alpha_p E'$$ (Loewenthal & Zaretsky, 1985) equation 8

Where α_p =2.6x10^{-8} Pa^{-1} represents the pressure-viscosity coefficient of the traction fluid (Santotrac 50).

The dimensionless central EHD film thickness is calculated as:

$$H_c = 2.69\, U_D^{0.67} G^{0.53} W^{-0.067}(1 - 0.61e^{-0.73k})$$ (Loewenthal & Zaretsky, 1985) equation 12

The central EHD film thickness h_c is calculated from:

$$H_c = \frac{h_c}{R_x}$$ (Loewenthal & Zaretsky, 1985) equation 2

The rolling traction power loss is calculated as:

$$P_r = 9 \times 10^7 h_c l U$$ (Loewenthal & Zaretsky, 1985) equation 2

Where the length of line contact $l = 2a$

Hysteresis power loss

The hysteresis power loss is calculated as:

$$P_h = F_h U = \frac{3}{16} \varphi \frac{b}{R_x} QU$$ (Loewenthal & Zaretsky, 1985) equation 51 and page 38

Where the hysteresis loss factor for steel is φ=0.01

Total power loss and power efficiency

The total power loss is calculated as:

$P_{loss} = P_C + P_t + P_h$

The percentage power efficiency is calculated as:

$P_{eff}=100(P_t- P_{loss})/ P_t$

h) Surface finish calculations

The ratio of film thickness to composite roughness, λ is set to 2 to avoid surface distress. The composite roughness σ is then calculated from:

$\lambda = h_C/\sigma$ (Loewenthal & Zaretsky, 1985) page 38

Therefore the actual composite surface roughness should be less than above calculated σ.

Assuming equal surface roughness, R_{Aq}, of body A and R_{Bq}, of body B, the maximum surface roughness, R_q, of body A and B is calculated from:

$R_q=(\sigma^2/2)^{0.5}$ (Leimei, 2013) equation 2

Where $\sigma = (R_{Aq}^2+ R_{Bq}^2)^{0.5}$

Matlab code was generated to calculate above. The Matlab results were compared against the Performance calculation example in section 3.3 of (Loewenthal & Zaretsky, 1985) page 35 to 38 to ensure correctness.

The use of the regression analysis is valid for the parameter ranges in Figure 7 below.

σ_0, GPa ..... 1.0 to 2.5
U, m/sec ..... 1.0 to 100
$\tilde{T}$, °C ..... 30 to 100
k ..... 0.5 to 8
$\omega_s\sqrt{ab}/U$ ..... 0 to 0.04

Figure 7 Regression analysis parameter ranges

4 Matlab simulation results

Matlab results are presented in the form of graphs, each including the relevant results for both body A and body B(Convex disk) and for body A and body C(Concave disk).

Since all current commercial CVT and developmental CVT include a variable input radius, a complex hydraulic control/clamping system is used to vary Q when the input radius varies. This is required since the tangential contact traction force changes (assuming input torque is unchanged) as the radius changes. What complicates the matter even further is that two contact friction drives, including at least two variable radii needs to be optimised by a single clamping mechanism in toroidal CVT's. In belt CVT's two clamping actuators is used, one at each pulley, but need to be synchronised to maintain the current ratio as torque demand changes. Controlling slip seems to be a dominant control strategy in current commercial and developmental CVT's. Referring for example to (Jans, 2005), the Cone Ring CVT performs at maximum traction coefficient at 2% slip and the control system was developed to maintain this level of slip. Control can be simplified to account for torque changes by using a loading cam. The variable surface rolling speed in commercial and developmental CVT's adds yet another layer of complexity to the control system, since all of them create a very significant overdrive in high ratio, resulting in component speeds of more than double engine/input speed, with the resulting increase in rolling surface speed and the subsequent drop in traction coefficient thus requiring a higher clamping force, Q, to maintain current torque transfer levels. This also leads to more contact cycles and reduces life of the components. As an example typical operating traction coefficients reported by Torotrak (Heumann, Briffet, & Burke, 2003) varied from 0.035 to 0.055. All current commercial and developmental CVT's have two friction interfaces in series, resulting in compounded losses.

The RADIALcvt has two very significant fundamental advantages in comparison to above.

- **Only one friction contact**: The RADIALcvt has only one friction drive contact in series in its parallel power paths and there are therefore no compound losses.
- **Constant rolling speed**: The maximum surface rolling speed U, is constant through the ratio range for a given input rpm and is very low at a maximum of 14.3 m/s. Thus for engine input from idle to 4400 rpm, U changes from 3.25 m/s to 14.3 m/s. Figure

5 indicates that above rolling speed range is on the left hand side and will therefore not contribute in the reduction of the maximum traction coefficient as is the case in commercial and developmental CVT's

4.1 Traction curves, spin and max traction coefficient

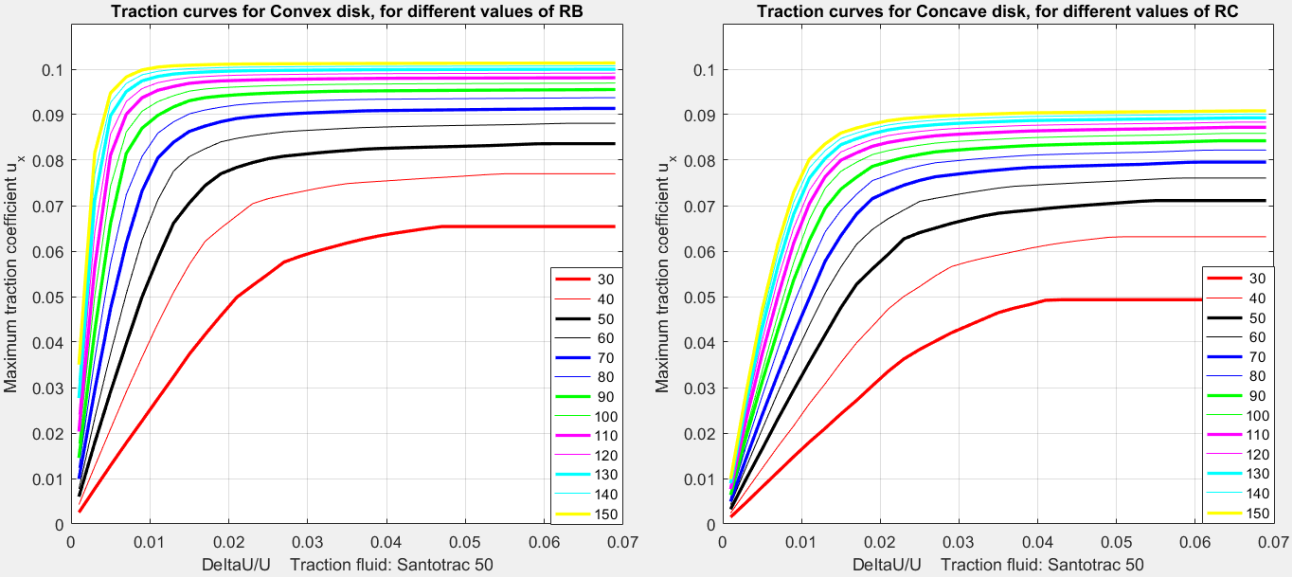

Figure 8 Traction curves

Figure 8 presents the traction curves for the Convex (R_B) disk and Concave(R_C) disk for different values of R_B and R_C. It can be seen that on average the maximum traction coefficient is 0.01 lower in the Concave disk in comparison to the Convex disk. Also small disk radii result in low maximum traction coefficients which exponentially increase with an increase in disk radius. Typically increasing the minimum disk radius from 30mm to 40mm will result in an about 0.013 increase in the maximum traction coefficient.

Evaluating Figure 9 and Figure 10 the following can be concluded:

- From the power loss contribution presented in Figure 10 is can be seen that the Traction contact power loss P_C is the only major contributor to power loss. P_C is a function of the loss factor LF which is a function of J_4, J_3 and k. Of these parameters, J_3 dominates and is directly related to spin via (Loewenthal & Zaretsky, 1985) equation 39 and also as reported by (Lichao, 2013).

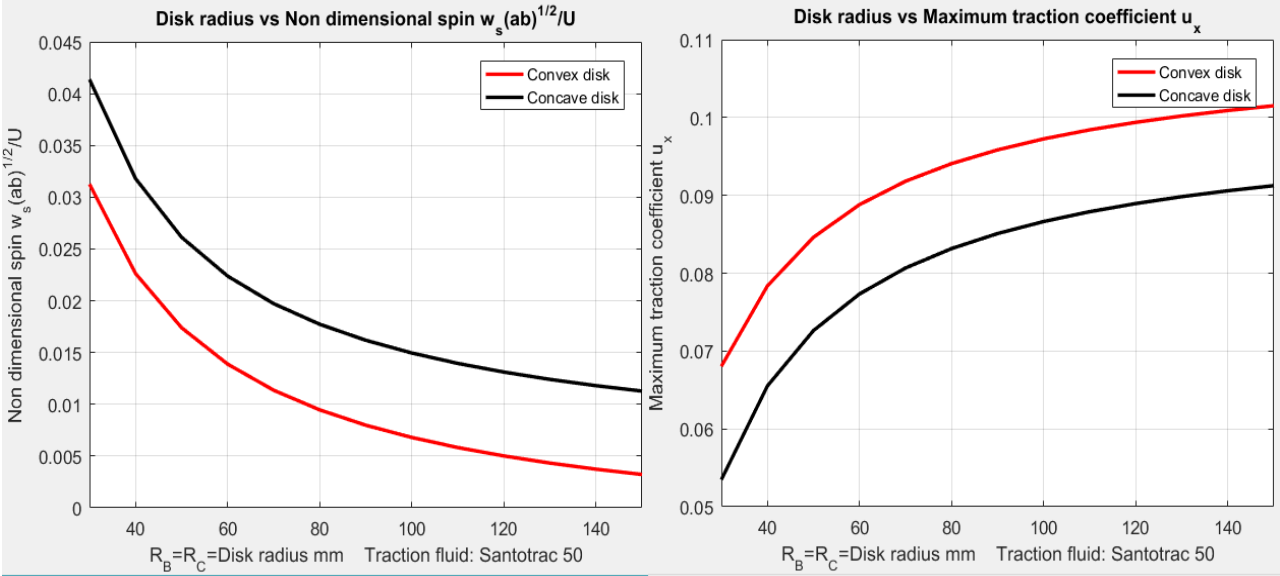

Figure 9 Spin and maximum traction coefficient

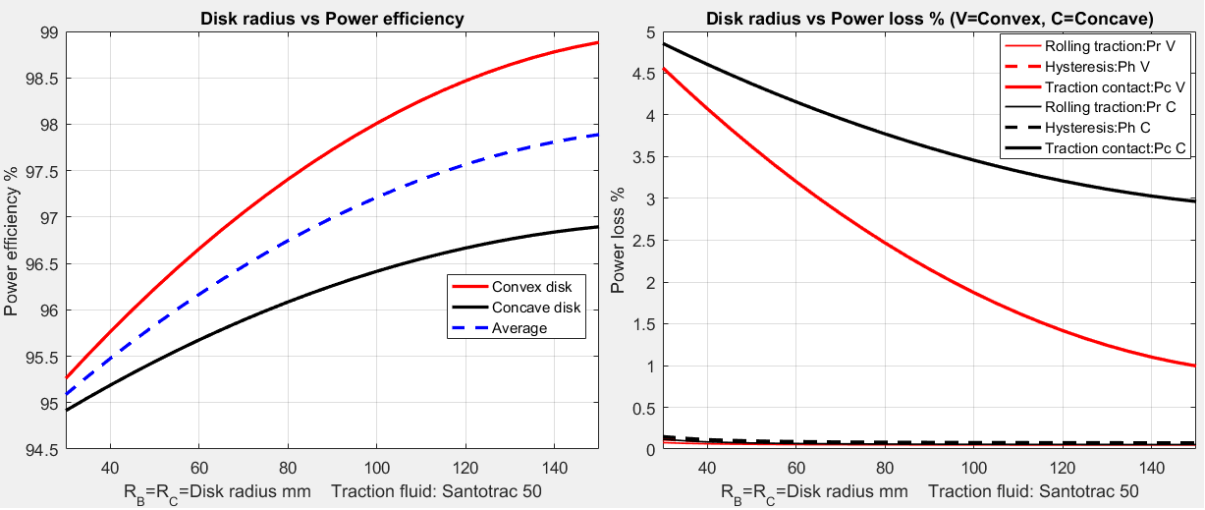

Figure 10 Power efficiency and power losses

- The source of spin, ω_S, is the result of a mismatch in body A and body B radii at contact points on either side of the point of pure rolling and is calculated by

$$\frac{\omega_S}{U} = \frac{\sin\theta}{R_A} - \frac{\sin(\gamma-\theta)}{R_B}$$

as presented in section 3.4. Spin is zero when the line tangent to the contact point intersects the intersection of the rotating axes of body A and body B. Therefore if spin needs to be reduced at the low disk radii then for the convex disk, Θ_B need to be increased at these radii or R_A needs to be decreased and/or R_B increased. (Assuming close to equal R_B and R_A then $\Theta_B = 45^0$ will result in zero spin)

Similarly, for the concave disk, spin can be reduced by decreasing R_A and/or increasing R_B or in this case, Θ_C being negative, needs to be less negative or positive.

- However the radial adjustment of body A (to adjust the ratio) is dependent on a disk angle. If the disk angle is zero ($\Theta_B = \Theta_C = 0$) then the axis of body A needs to be at an angle other than 90^0 to the axes of body B and C in order to shift ratios. This will represent the only configuration in which the performance of the two disks is identical. Performance optimisation will therefore include the comparison of the combined performance of the convex and concave disk when Θ_B and Θ_C are not equal, to the configuration where body B and body C are flat disks while body A axis is at an angle other than 90^0 to the axis of body B and C. The current first prototype will provide a lot of insights into its shifting characteristics.

- To counter the effect of the lower maximum traction coefficient at low R_B and R_C the profile of the convex disk and concave disk can be modified to have a variable angle Θ_B and or Θ_C angle in such a way as to decrease the distance between these disks at low values of R_B and R_C. The effect will be that the two disks will be forced further apart when body A makes contact in this region. Since the clamping force is supplied by mechanical springs, the springs will be further compressed and the clamping force will increase accordingly to maintain the current torque level by compensating for the lower maximum traction coefficient. For example the current prototype springs are compressed 4mm, thus if above method is applied and for example if the springs are just compressed an additional 1mm this will result in a 25% increase in the clamping force.

- It is also very important to note that the high R_B and R_C values correspond to the low RADIALcvt ratios at pull away. Thus in city driving the RADIALcvt will operate in its very high power efficiency range typically under lower power loads. Current commercial CVT have difficulty in obtaining high power efficiency in these conditions, particularly because of the hydraulic control system.

- Thus for a very basic RADIALcvt, assuming low maximum contact stresses, typically below 2 GPa, the clamping force can be constant and thus created by mechanical springs. This however will result in over clamping at partial load, but the associated efficiency loss needs to be compared to the cost of a loading cam.

- When a more powerful RADIALcvt is considered, the same basic design is used, and maximum clamping force can be increased to say 2.5 GPa while employing a loading cam in combination with mechanical springs to optimize clamping vs input torque. This loading cam can be based on input torque as presented in section 4.3.5.

4.2 Elliptic ratio, maximum contact stress and power efficiency

The elliptic ratio k, a and b plays an important role in both the maximum contact stress and spin. Ideally a high value of b (semi width of contact area in the x or rolling direction) is desired with lower values of a (semi width of contact area in the y- direction transverse to the rolling direction) to produce lower values of k=a/b. However the larger the area created by the ellipse with radii a and b the lower the maximum contact stress. Line contact between body A and B as well as A and C is very effective in reducing the maximum contact stress. However line contact is only possible throughout the ratio range for constant values of Θ_B and Θ_C while this line contact l=2a is in the y direction, so care should be taken that it does not have a significant effect on increasing spin losses.

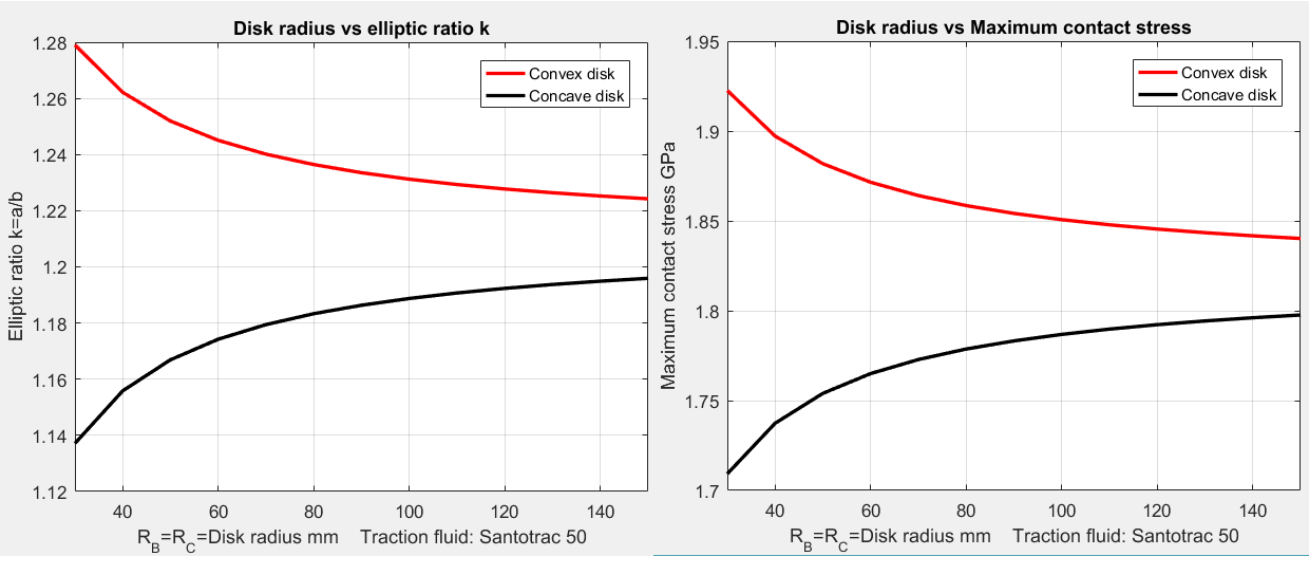

Figure 11 Maximum contact stress and elliptic ratio

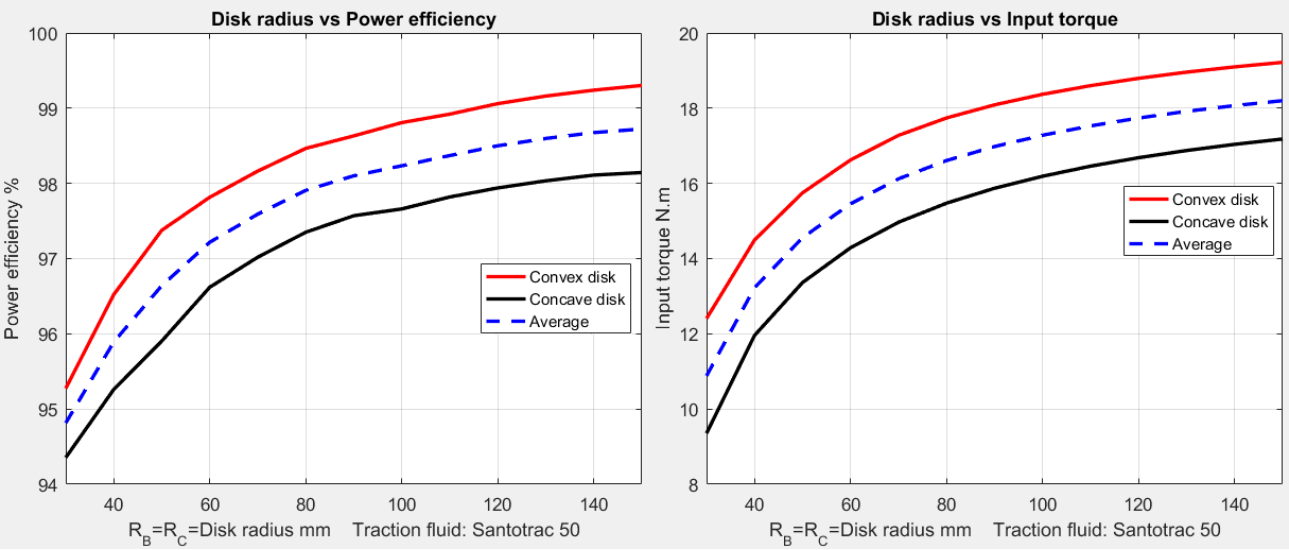

Figure 12 Power efficiency and Input torque

Evaluating Figure 11 and Figure 12 the following conclusions can be made:

- The convex disk produces higher k and maximum contact stresses while all stresses is below 2 GPa in the current design.
- Power efficiency is generally very high, average from about 95% to 98.5%, with the convex disk typically 1% higher than the concave disk.
- Average torque increase from low values of R_B and R_C from about 11 N.m to 18N.m while the Convex disk torque is generally about 2 N.m higher.
- Note the total torque of the current RADIALcvt is obtained by multiplying above average torque by the 6 parallel power paths, thus from about 66 N.m to 108 N.m. and 30 kW to 50 kW Figure 13 presents the input power and torque of the complete RADIALcvt.

Figure 14 presents the central film thickness h_c and the minimum surface roughness R_q for above conditions. It can be seen that a surface roughness of about 0.4 um on both the radial driver and disks will prevent metal on metal contact.

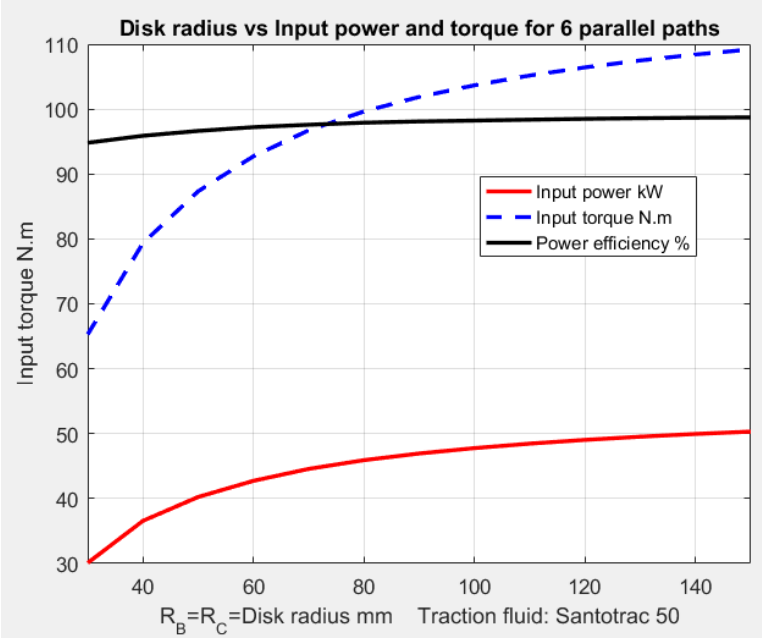

Figure 13 Input power, torque and power efficiency for the complete RADIALcvt

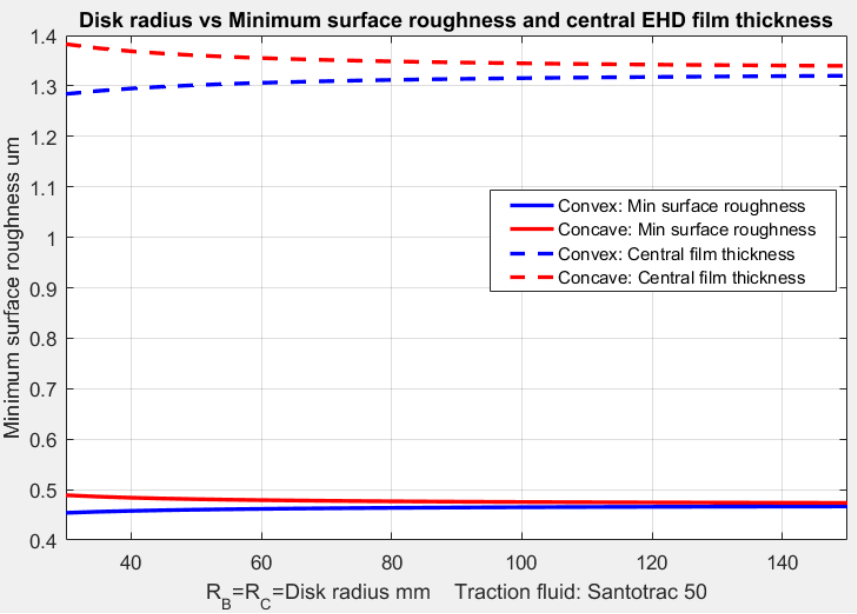

Figure 14 Minimum surface roughness and EHD film thickness

4.3 Comments on optimization

4.3.1 Increasing maximum disk size

The current RADIALcvt has a disk diameter of 292mm. In the case of a front wheel drive transmission the standard is that the differential axis is 180mm from the engine/RADIALcvt input axis. If it is assumed that a 25mm driveshaft has to pass over the disks, the disk diameter can be increased to 335 and typically the R_B and R_C range can be increased from

143mm to 165mm. If a ratio range of 4.5, equal to the current equivalent manual transmission is chosen, the minimum value of R_B and R_C will increase from 30mm to 37mm. Above results in a 0.5% increase at the minimum value of R_B and R_C in power efficiency from 95% to 95.5%.

4.3.2 Varying planetary system e value

From Figure 12 it can be seen that the input torque of the Concave disk is consistently lower than that of the Convex disk. If left unattended, the Concave disk torque will always represent the maximum input torque for both the Concave and Convex disk for an equally balanced planetary system with e value of -1 if calculated according to (Shingley & Miscke, 1989) page 553, which results in an equal 50% torque contribution of both the Convex and Concave disk to the Combining planetary system of Figure 1. By changing the e value of the Combining planetary system the torque contribution between the Convex and the Concave disk can be changed to such a ratio as to compensate for the difference in maximum toque capability of the two disks. Such a non-equal ratio will allow each disk to produce its respective maximum torque for the same clamping force. (Shingley & Miscke, 1989)

4.3.3 Integrating a two speed AMT

If a more power full RADIALcvt is considered and if it needs to compete with the current maximum ratio range on the market, around 10, then the following can be done:

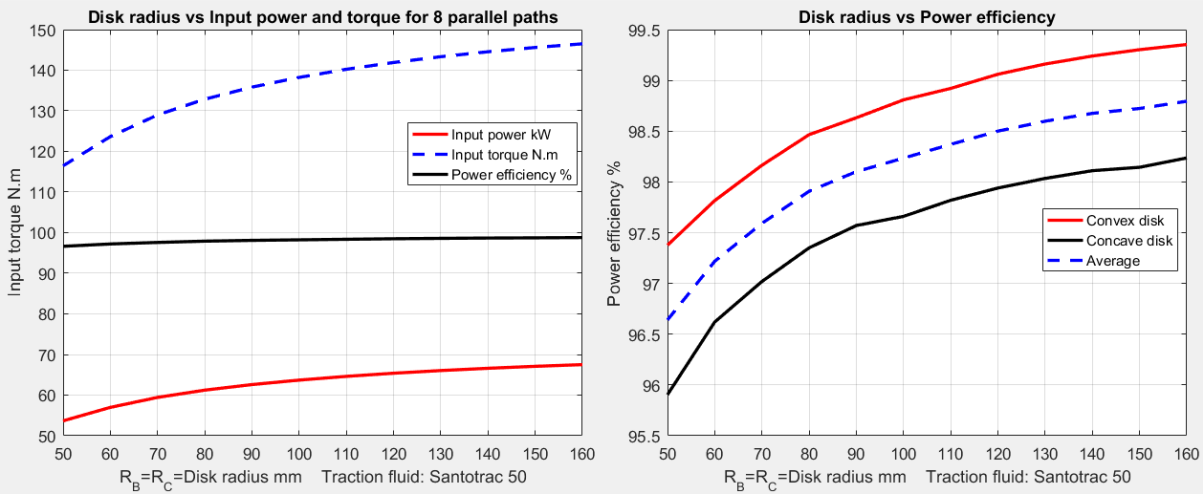

Figure 15 Effect of 2 speed AMT integration

- A two speed automated manual transmission can be integrated and this will require the RADIALcvt variator to only produce a ratio range of $10^{1/2}$=3.16.

- Taking above maximum R_B and R_C value of 165 and ignoring the fact that a more powerful engine will have a bigger flywheel and therefore allow bigger disks, the operating range of R_B and R_C is decreased to 165/3.16=52.2 to 165 mm.
- Above will create space around the input bevel gear and will allow the addition of another radial drive (body A) resulting in 8 parallel power paths vs the current 6.

Figure 15 presents the results of above with minimum power efficiency of about 96.6% in high ratio to about 98.7% in low ratio.

4.3.4 Increase line contact length

Increasing the line contact from 2.35 mm to 5 mm reduces the maximum contact stress, but increase a and therefore also k which leads to an increase in spin and lowering the power efficiency. Increasing the normal load Q to 15600 N, still produces contact stresses below 2 GPa but increases minimum input torque and power to 225 N.m and 100 kW respectively as presented in Figure 16. Above is accomplished with the sacrifice of about 1.25 % in minimum power efficiency of which the average is still above 95 %. The huge advantage is the input torque and power is about double the levels before the line contact increase as presented in Figure 15.

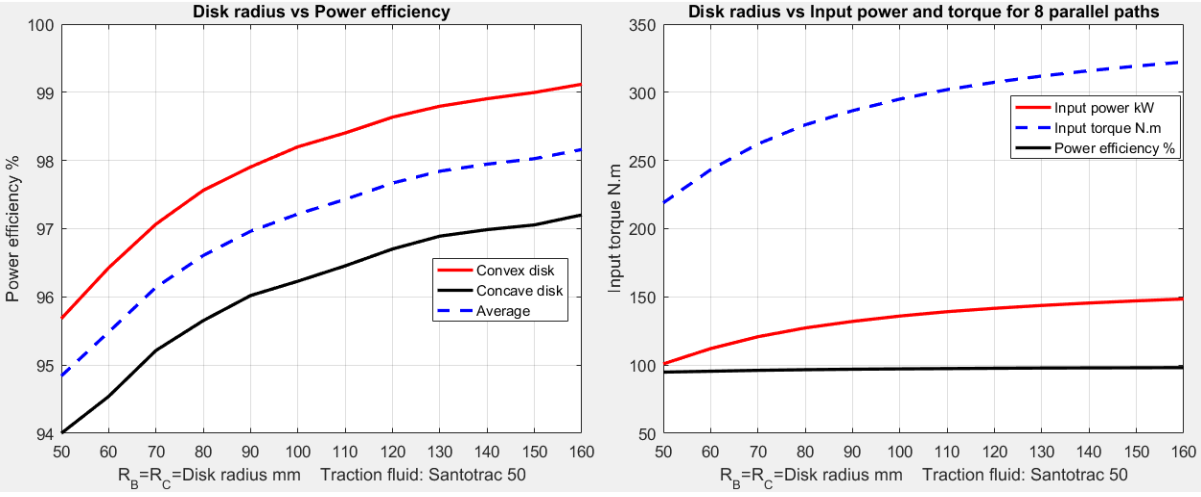

Figure 16 Effect of 2 speed AMT integration and line contact length increase

From Figure 17 it can be seen that spin level decrease as a result of the AMT integration (increase in the minimum R_B and R_C values), but again increased with the line contact length increase to more or less the same levels as that of Figure 9.

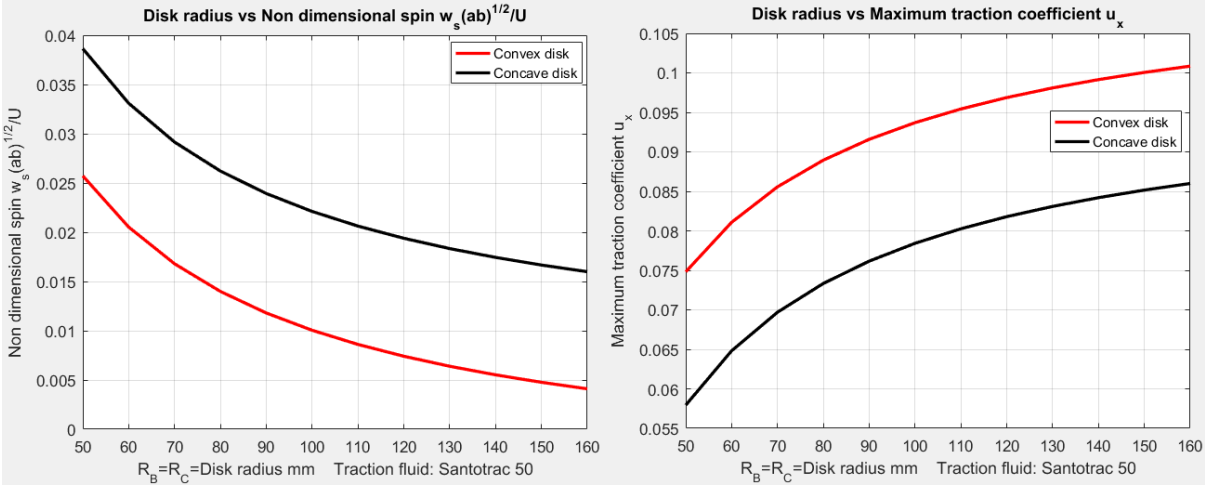

Figure 17 Line contact increase effect on spin and maximum traction coefficient.

4.3.5 Different Θ angles and a loading cam

Note that line contact are maintained, if different fixed angles of Θ_B and Θ_C are used, while this difference will create a variable normal load Q, created by mechanical springs, which can be used to compensate for the lower maximum traction coefficient at low R_B and R_C values. This will then also prevent over clamping in high values of R_B and R_C. Note that all of above is based on maximum contact stress values of less than 2 GPa, which is very low compared to industry standards.

In case where over clamping due to partial loads occur, the cost penalty to implement a loading cam need to be considered and compared to the power efficiency gain.

The configuration of the RADIALcvt variator facilitates the implementation of a loading cam in the following way. The structure, in which the radial drivers are housed, has a reaction torque around its axis (coinciding with the axis of the input shaft) which is equal to the input torque. The reason for this being the fact that each radial driver (body A) is subject to a tangential traction force in each of the two contacts with the convex a concave disk. These forces are substantially equal but in opposite directions, thus cancelling each other.

Thus for the implementation of a loading cam the above structure, housing the radial drivers, can be coupled (which may include a torque multiplying gear ratio) to a loading cam operation between one of the disk bearings and the RADIALcvt casing.

With above in place the combination of different fixed angles of Θ_B and Θ_C together with mechanical springs and the addition of a loading cam as per above would prevent over clamping in all operating conditions of the RADIALcvt.

5 Contact simulation summary

In general considering the high levels of power efficiency which should result in low operating temperatures and relative high maximum traction coefficients at relative low maximum contact stresses (below 2 GPa) the following:

- Other traction fluids should be investigate that under low temperatures and low contact stresses provide better maximum traction coefficients at higher levels of spin. (Loewenthal & Zaretsky, 1985) indicates that softer traction fluids (lower slope m) with thicker film thickness are more tolerant of spin.
- Note that all of above is under the assumption that engine torque and power does not need to be limited in some ratios as is the case with commercial CVT's. Therefore the RADIALcvt relies on the fact that it can, in all ratios, handle any maximum torque the engine can create, thus eliminating any engine power or torque limiting control system.

5.1 Without AMT integration

Without AMT integration, the spin levels are already high and therefore any contact line increase will further lower the maximum traction fluid and power efficiency. The performance of the contact line in question does not vary too much from a crowned surface in terms of contact stresses, thus in this case variable Θ_B and Θ_C angles can be used to counter spin and vary clamping force to compensate for lower maximum traction coefficient. Ratio range for the current prototype is 4.7 and seems to be close to a maximum because of the available space. Minimum power and torque levels are at 30 kW and 66 N.m respectively.

5.2 With 2 speed AMT integration

With AMT integration the ratio range is reduced to 3.16 to provide a CVT with an overall ratio range of 10, equalling the maximum currently in the industry. The reduced ratio range,

enables larger minimum R_B and R_C values which in turn reduce spin, increase traction coefficient and power efficiency while also allow space for the inclusion of a fourth radial drive (body A) thus creating 8 parallel power paths.

If Θ_B and Θ_C are kept fixed, line contact is possible in all ratios and by increasing the line contact reduces the maximum contact stress. The downside of line contact is an increase in spin, resulting in lower maximum traction coefficient and lower power efficiency.

However by increasing the contact line length from 2.3mm to 5mm and increasing the normal load Q to 15600 N, while still keeping maximum contact stresses below 2 GPa, produces a 225 N.m, 100 kW CVT with a minimum power efficiency of 95 %. The penalty for the line contact increase is about 1.25 % in power efficiency. Note that line contact is not possible in toroidal or planet ball CVT's. This is thus a major advantage of the RADIALcvt.

Yet another advantage of the RADIALcvt in comparison to chain/belt CVT's is the fact that the disks in the RADIALcvt are uniformly loaded. In chain/belt CVT's the chain/belt only makes contact on the one side of the disks creating a force that tends to push the disks away from each other on only one side. To counter this involves stiffer disks, shafts and bearings to deal with this.

Yet another advantage of the RADIALcvt compared to current commercial and developmental CVT's is the fact that in the case of the RADIALcvt, one unit of clamping force supports 2 parallel power paths. In the case of toroidal and planet ball CVT's a unit of clamping force support two friction drive contacts point (input toroid to roller to output toroid) of a single friction drive path with two friction drive contacts in series. In belt/chain CVT's for the input pulley a unit of clamping force supports two friction contact interfaces on either side of the belt/chain which represents two parallel power paths, but since an output pulley is also required the total belt/chain CVT with two pulleys and their respective clamping forces also result in two friction drive interfaces for each unit of clamping force, the same as for the toroidal CVT's. However note that in belt/chain CVT's the clamping force is not applied across bearings, thus they do not suffer the effect of bearing loss due to clamping force. However the camping force creates a belt/chain tension force which tends to pull the two pulleys towards each other and therefore the bearings being loaded with this force suffer the relevant losses indirectly caused by the clamping force.

In high efficiency traction drives, the losses in the bearings supporting the clamping force can be a major contributor to the overall losses in the CVT (Loewenthal & Zaretsky, 1985). Above provides the RADIALcvt with a fundamental advantage with the potential of having only 50% of the clamping bearing losses if compared to belt/chain, toroidal, planet ball and cone ring CVT's.

6 Bearing loss analysis

6.1 Disk bearings

The disk bearings presented in Figure 1 is for use in a RADIALcvt display version with perspex casing plates and is not suited for efficiency testing because of their large diameter which will result in large bearing losses. Disk bearing in use for efficiency testing will typically be much smaller diameter taper roller or ball thrust bearings. Bearing losses are calculated from the SKF bearing manual (SKF, 1989) as follows:

Load-independent frictional moment (due to lubricant hydrodynamic losses):

$M_0=10^{-7}f_0(Vn)^{2/3}dm^3$ N.mm for Vn> 2000

$M_0=160x10^{-7}f_0dm^3$ N.mm for Vn< 2000

Load dependent frictional moment (due to elastic deformation and partial sliding):

$M_1=f_1P_1{}^a dm^b$ N.mm

Where

dm= mean diameter of bearing 0.5(ID +OD) mm

V= kinematic viscosity of lubricant mm^2/s

n= bearing speed rpm

f_0 = bearing factor and lubrication type according to Table 2 (SKF, 1989).

f_1 = bearing type and load factor according to Table 2 (SKF, 1989).

P_1= the load N determining the frictional moment according to Table 3 (SKF, 1989).

For all bearings under consideration a=b=1.

PM_0 and PM_1 represent the power losses as a percentage of transmitted power associated with torque losses M_0 and M_1 respectively.

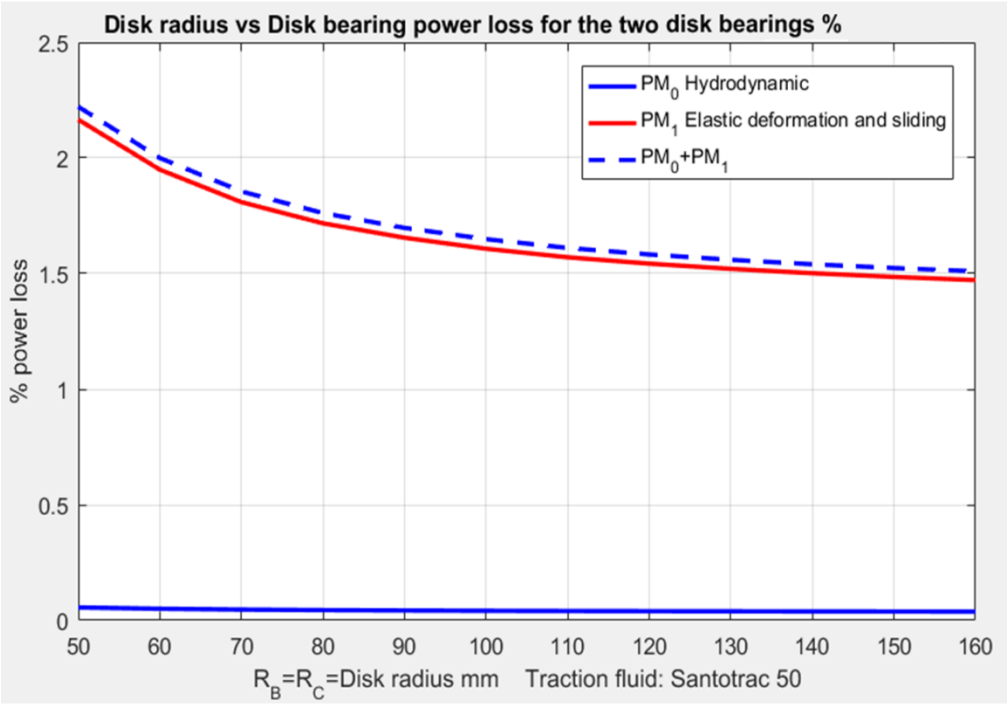

Figure 18 Disk bearing loss: AMT integrated and extended contact line.

For use in both the convex and concave disk, for the AMT integrated case with longer contact lines, a SKF 32013 taper roller bearing with ID=65 mm and OD=100 mm is chosen (basic load rating: dynamic 84 200N, static 127 000N). Note this bearing is able to handle the increased normal force Q = 15600 N as used in section 4.3.4. The total normal force for this scenario with 8 parallel power paths is 4x15600 N = 62400 N. Figure 18 presents the above load independent and dependent frictional moments M_0 and M_1 respectively as a percentage power loss PM_0 and PM_1 respectively, for the conditions as presented in Figure 16 and Figure 17.

From Figure 18 it can be seen that the load dependant elastic deformation and partial sliding loss PM_1 dominates the PM_0 loss and that the loss is a maximum of about 2.3 %.

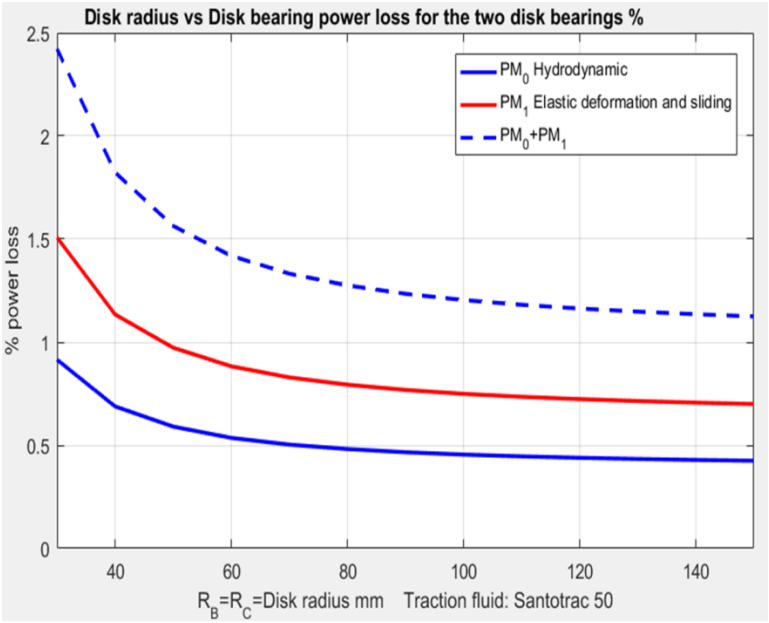

Figure 19 Disk bearing loss: Basic case without AMT integration.

For use in the convex and concave disk, the case without an AMT, a SKF 51113 thrust ball bearing with ID=65 mm and OD=90 mm is chosen (basic load rating: dynamic 37 000 N, static 98 000 N). Note this bearing is able to handle the normal force Q = 6800 N as used in section 4.1. The total normal force for this scenario with 6 parallel power paths is 3x6800 N=20400 N. From Figure 18 it can be seen that each of the losses PM_1 and PM_0 contribute and that the loss is a maximum of about 2.4 %.

It can thus be concluded that overall disk bearing losses, under the influence of the clamping force, is at a maximum of less than 2.5 %

6.1.1 Clamping force advantages

The RADIALcvt configuration includes the following two important clamping force advantages.

- **Clamping force utilization:** As already mentioned in section 5.2, a unit of clamping force supports two parallel friction interfaces, and all other CVT's supports only one, thus in equal conditions the RADIALcvt should have 50% of the clamping bearing losses.
- **Clamping force location:** The RADIALcvt clamping force, bearing losses are only associated with the RADIALcvt output, namely the Convex and Concave disks, while the RADIALcvt input, the radial drivers, are in equilibrium as mentioned in section

4.3.5. Thus these bearing losses, for a given clamping force, are only a function of the RADIALcvt output speed. This has the obvious low loss advantages in low output speed ratios. In contrast in all other CVT's, the clamping force is associated with both the input and output speeds of the respective CVT, thus for a given clamping force the applicable speed for bearing loss calculation would be the average of the input and output speeds.

6.2 Radial shaft bearing losses

As described in section 4.3.5 the radial shafts experience no radial load as a result of its interaction though the two friction drive contacts as the tangential forces cancel out. Thus the bottom radial bearing experience the radial and axial force created in its 1:1 zerol bevel drive with the input shaft. Using the equation provided by (TIMKEN, 2017) the tangential force and axial thrust of the Zerol gear is calculated and used as input in the bearing loss calculations. Figure 20 presents the losses for the conditions of Figure 19 and it can be seen that these losses can be ignored.

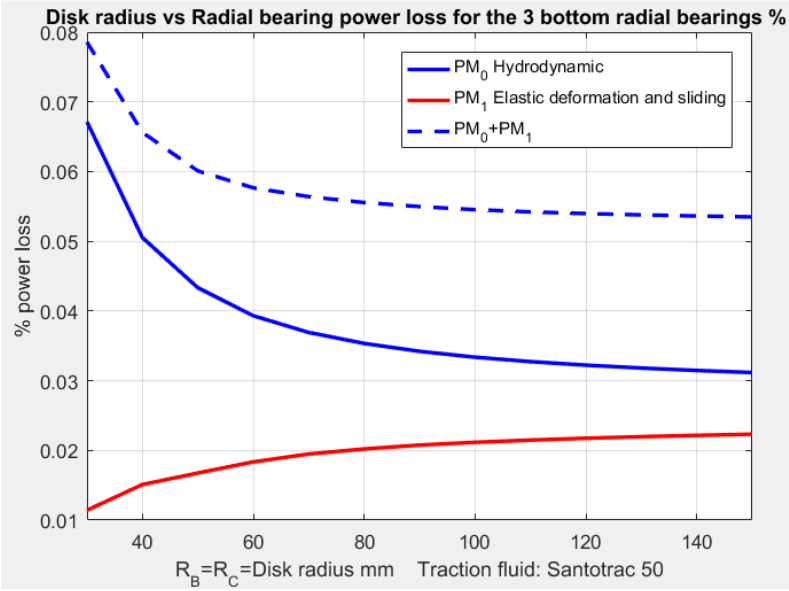

Figure 20 Bottom radial driver bearing losses.

Note that above bearing selection are not optimised in any way. Investigation into different bearing sizes and types should lower the bearing losses further.

7 Ratio shifting analysis

7.1 Geometry analysis

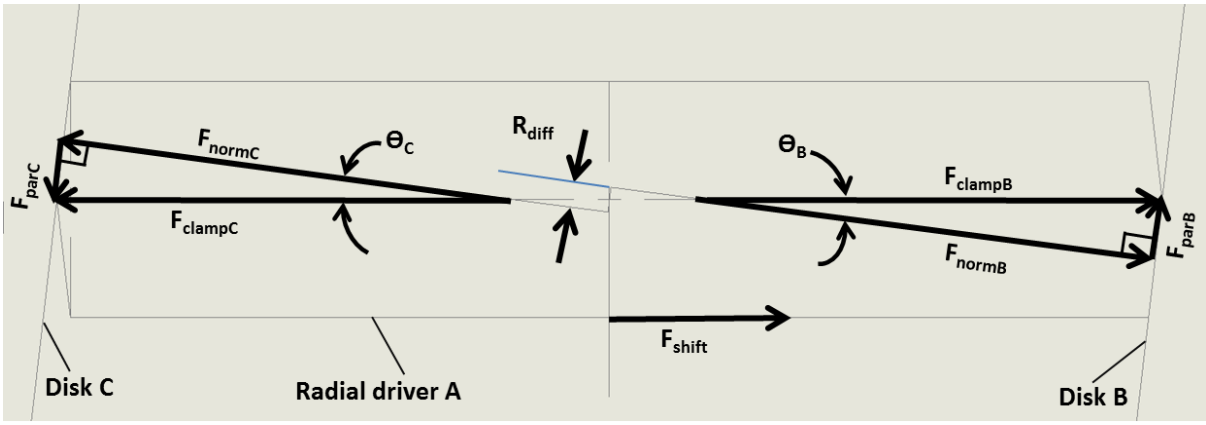

Figure 21 Radial driver force diagram

Figure 21 presents the two force diagrams on the radial driver as a result of the Convex disk (B) and Concave disk (C) being clamped together by a force F_{clampB} which under normal operating conditions is equal to F_{clampC} resulting in line contact between the two disks and the Radial driver. It is assumed that the normal force (F_{parB} and F_{parC}) between the respective disk and Radial driver act at the centre of the contact line. Disk B convex angle is Θ_B and disk C concave angle is Θ_C and is currently taken as being equal.

The force F_{shift} acts perpendicular to the radial driver axis and is the result of moving the radial driver shaft in the direction of F_{shift} during ratio shifting, thus to a larger radius of R_B and R_C.

The following relationships can be established from Figure 20 and above.

$$F_{parB} = (F_{clampB} + F_{shift})\sin(\Theta_B) \quad (R1)$$

$$F_{parC} = (F_{clampC} - F_{shift})\sin(\Theta_C) \quad (R2)$$

The difference between the vertical components of F_{parB} and F_{parC} provides the resultant force shifting F_S which will be exerted on the radial driver to move it to a different radial ratio position. Thus from above

$$F_s = F_{parB}\cos(\Theta_B) - F_{parC}\cos(\Theta_C) \quad (R3)$$

Combining equation 1 to 3 provides

$$F_S = \cos(\Theta_B)(F_{clampB} + F_{shift})\sin(\Theta_B) - \cos(\Theta_C)(F_{clampC} - F_{shift})\sin(\Theta_C) \quad (R4)$$

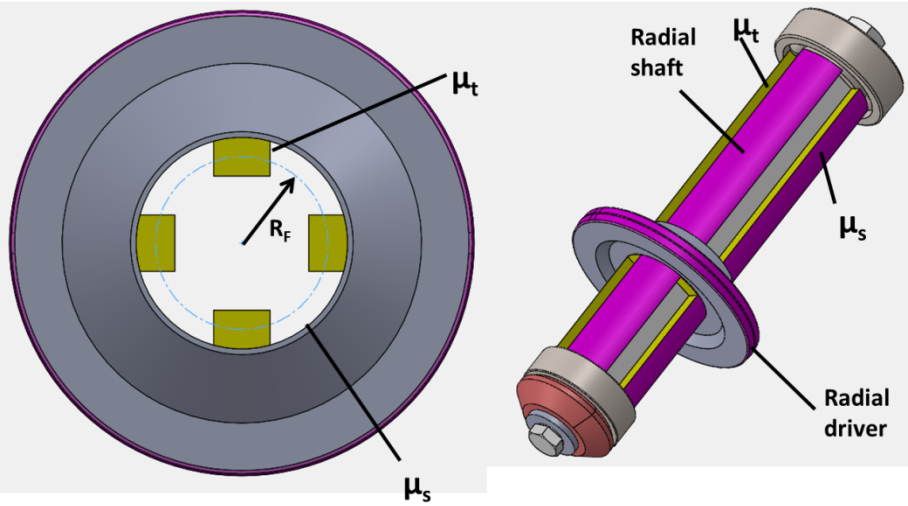

Figure 22 Radial shaft and driver

In order to shift, F_S needs to be larger than F_{fric}, the friction force with friction coefficient μ_t between the radial driver and radial shaft created by the torque T_t being transmitted, added to the friction force with friction coefficient μ_s between the radial driver and radial shaft created by F_{shift}, thus:

$$F_{fric} = T_t \mu_t / R_F + F_{shift} \mu_s \quad (R5)$$

In order for the current ratio to be in equilibrium, F_S, in equation R4 is set to zero and solving for F_{shift}, while noting that $F_{clamp} = F_{clampB} = F_{clampB}$ =clamping force across disks, gives:

$$F_{shift} = F_{clamp}\,[\cos(\Theta_C)\sin(\Theta_C) - \cos(\Theta_B)\sin(\Theta_B)]/[\cos(\Theta_B)\sin(\Theta_B) + \cos(\Theta_C)\sin(\Theta_C)] \quad (R6)$$

From equation R6 is can be seen that F_{shift} is only zero if $\Theta_C = \Theta_B$, thus if they differ F_{shift} will represent the force required to keep the RADIALcvt in the current ratio.

The radial driver also experiences a torque T_D around an axis perpendicular to Figure 21 as a result of the distance R_{diff} and it is calculated by:

$$T_D = 0.5 R_{diff}(F_{normB} + F_{normC}) \quad (R7)$$

In terms of the clamping forces, equation R7 can be written as:

$$T_D=0.5R_{diff}(F_{clampB}\cos(\Theta_B) + F_{clampC}\cos(\Theta_C)) \quad (R8)$$

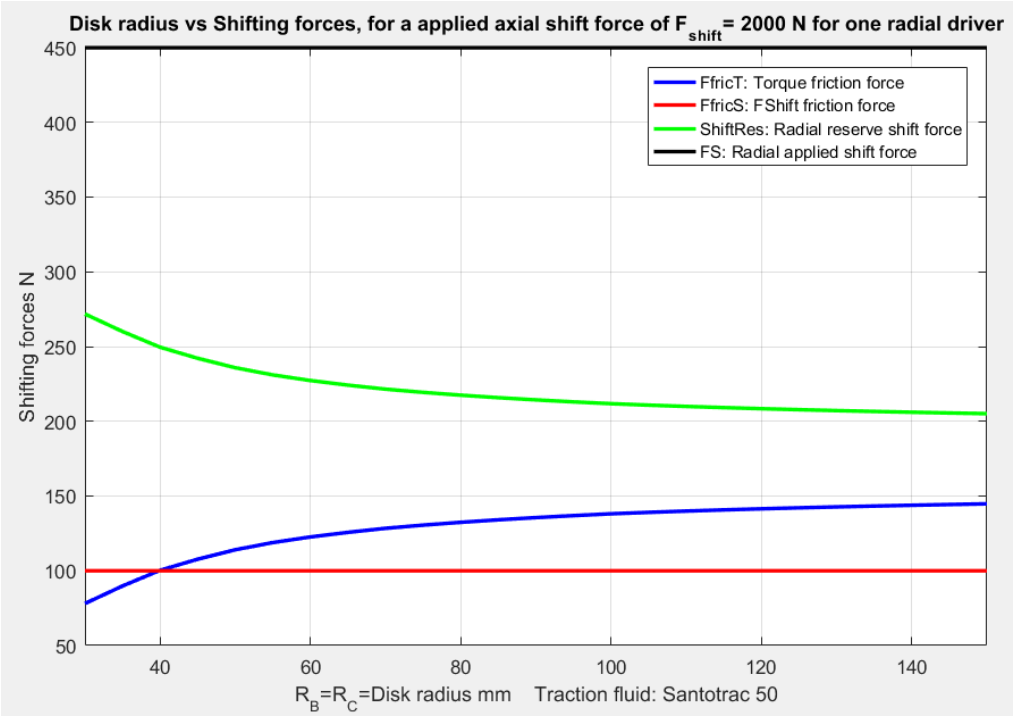

Figure 23 Ratio shifting forces

Figure 23 below present the ratio shifting parameters for the conditions presented in Figure 8 to Figure 13 with $\mu_t = \mu_s = 0.05$. It can be seen that ShiftRes= F_S- $F_{fric,}$ has positive values thus the shifting force F_{shift}=2000 N will be sufficient to overcame the friction. ShiftRes thus represents the force available to act on the two rolling friction drive contact interfaces, on either side of the radial driver, to move it to a larger radius/values of R_B and R_C. The rate of this radius change will be further investigated when experimental data is available, but should be a function of clamping force and torque transmitted.

The moment T_D as calculated from equation R8 might also have an effect on μ_t and μ_s as it might tend to continually close the tolerance gap between the radial driver and radial shaft on opposite sides in an axial direction of the radial driver and will also be investigated when experimental data is available. Shifting friction force can be drastically reduced by implementing ball splines between the radial shafts and the radial drivers. In this case μ_t and μ_s will represent rolling friction which is much lower than the above values of 0.05 for sliding friction, but the additional cost penalty need to be considered.

7.2 Total shifting torque and forces

The total torque V_t on the variator and the ball screw shifting force F_{bs} for the sum of all the radial drivers due to F_{shift} is calculated as follows:

$$V_t = F_{shift}\, n_{rd} L_{ramp}/(2\pi) \quad \text{(R9)}$$

$$F_{bs} = V_t/R_{bv} \quad \text{(R10)}$$

Where n_{rd} = number of radial drivers

L_{ramp} = the lead m/rev of the ramps on the casing on which the variator rides

R_{bv} =the radius from the RADIALcvt input axis to the ball screw attachment

Since F_{shift} is constant, V_t= 76 N.m and F_{bs}=381 N are also constant for the conditions in Figure 23. Note that as discussed in section 4.3, the normal force Q (directly related to the clamping force), which currently is constant, need to be varied, for optimization purposes, to allow a near constant input torque T_t. Thus if Q is not constant then F_{shift} will vary accordingly. Above values is only given as an example to present the order of magnitude.

8 References

Carter, J., Pohl, B., Raney, R., & Sadler, B. (2004). The Turbo Trac Traction Drive CVT. *SAE International*, 7.

Heumann, H., Briffet, G., & Burke, M. (2003). *System efficiency optimisation of the Torotrak Infinitely Variable Transmission (IVT).* Lancashire, UK.: Torotrak Development.

Jans, C. (2005). *Slip measurement and control in a cone ring transmission.* Eindhoven: Eindhoven University of Technology.

Leimei, L. (2013). *Assesment of Effects of Surface Roughness and Oil Viscosity on Friction Coefficient under Lubricated Rolling-sliding Conditions.* Komatsu.

Lichao, P. (2013). *Tribology of a CVT traction drive.* Eindhoven: Eindhoven University of Technology.

Loewenthal, S. H., & Rohn, D. A. (1983). *Regression analysis of traction characteristics of two traction fluids.* Cleveland, Ohio: NASA Technical paper 2154.

Loewenthal, S. H., & Zaretsky, E. V. (1985). *Design of Traction Drives.* Ohio: NASA Reference Publication 1154.

Loewenthal, S., & Rohn, D. (1983). Traction Behavior of Two Traction Lubricants. *American Society of Lubrication Engineers.* Houston, texas.

Shingley, J., & Miscke, C. (1989). *Mechanical Engineering Design* (Fifth ed.). Singapore: McGraw-Hill.

SKF. (1989). *SKF General catalogue.* Germany.

TIMKEN. (2017). *TIMKEN product catalog A21.*